A DFT Evaluation of Molecular Reactivity of Volatile Organic Compounds in Support of Chemical Ionization Mass Spectrometry

Manjeet Bhatia[1,2,⋆]

[1]Dipartimento di Fisica, Università degli Studi di Milano, Via Celoria, 16, I-20133 Milano, Italy
[2]Department of Food Quality and Nutrition, Research and Innovation Centre, Fondazione Edmund Mach, 38010 San Michele all'Adige, TN, Italy
⋆ Correspondence: manjeetbhatia83@gmail.com

Abstract

Gas-phase molecular properties of volatile organic compounds (VOCs) play an important role in the selection of gas-phase reagent ions for chemical ionization mass spectrometry (CI-MS). We apply hybrid density functional theory (DFT) to compute proton affinity (PA), ionization energy (IE), and global reactivity parameters for VOCs, which are widely regarded as the primary sources of taints and off-flavors in wine. Atomic polar tensor (APT) charges and total energies at the stationary point for neutral and protonated molecules are also computed. PA and IE values determine the CI-MS mode of reactions, either proton transfer or electron transfer from the reagent gas ions to VOCs. Global reactivity parameters, such as chemical potential (μ), chemical hardness (η), softness (σ), and electrophilic nature (ω) as obtained from frontier molecular orbitals, are considered useful in rationalizing the chemical reactivity patterns of the molecules. A benchmark calculation of indole molecule with MP2, B_3LYP, and M06-2X DFT methods at thermodynamically and kinetically stable protonation sites further supports the applied DFT method. Since limited data are available on computed parameters, the reported values would support CI-MS quantification of trace-level VOCs not only in wine but also in various food products.

I Introduction

The perception of aroma and flavor in wine is a complex interplay between numerous chemical compounds and sensory receptors (*1–3*). These aromas and flavor compounds, commonly ascribed as volatile organic compounds (VOCs), contribute to wine's unique texture and bouquet if present near the sensory threshold limits, however, excessive amounts can detract from the quality and are considered as a fault in wine (*4*, *5*). VOCs produce 'musty', 'moldy', 'wet floor', 'vinegar', and 'rotten egg' like off-flavors that generally appear during production and processing of wine. Among other common sources, the cork stopper of the wine bottle contributes to so-called 'cork-taint' in wine, causes significant losses to wineries (*6–9*). The identification of VOCs carrying taints and off-flavors and their accurate quantification in wine is critical in the assessment of the quality of the wine being produced. Due to their highly volatile nature and extremely low concentration, typically in part-per-trillion by volume (pptv) range, pose an analytic challenge in their identification and quantification (*10–12*).

Chemical ionization (CI) based direct-injection mass spectrometry (DIMS) techniques, such as proton transfer reaction mass spectrometry (PTR-MS) (*13*) and selected ion flow-tube mass spectrometry (SIFT-MS) (*14*) can reach the required accuracy and precision, as well as high throughput with a detection limit in the low pptv level is indispensable in the detection of taste and flavor (*15*, *16*). These ionization methods are generally based on the ionization of the neutral VOCs via commonly used reagent ions, such as H_3O^+, NH_4^+, NO^+ and O_2^+ ions. Furthermore, the ionization mechanism through different reagent ions and ion-molecule reaction kinetics relies on the chemical and physical properties of neutral VOCs (*17*).

Gas-phase molecular properties, such as proton affinity (PA), ionization energy (IE), and global reactivity parameters of the neutral VOCs are of utmost importance in the selection of appropriate reactant gas (ions) to be utilized in chemical ionization mass spectrometry (CI-MS) (*17*, *18*). PA of a neutral molecule determines whether a reaction proceeds by proton transfer, typically with H_3O^+ or NH_4^+, on fragmentation or adduct formation, as occurs in CI-MS. The H_3O^+ ion is key to proton transfer reactions in the PTR-MS because of its high abundance in combination with the low PA (*19*) i.e. 166.5 kcal/mol. An effective exothermic proton transfer occurs in such analyte molecules that possess higher PA than H_2O. If a reactant gas with lower PA than H_2O is selected, the proton transfer is followed by fragmentation, whose extent depends on the size of the PA difference between an analyte and the H_2O molecule. On the other hand, reactant gases with very high PA than H_2O often lead to adduct formation. Moreover, NH_4^+-CI-MS ionization is useful for effective proton transfer reactions wherein the PA of a molecule is higher than H_2O, typically by 23 kcal/mol (*20*).

The PA of a molecule in the gas phase can be determined either by relative methods, kinetic or thermo kinetic, a gas-phase equilibrium constant based upon some absolute standards that are accessible over ionization threshold measurements

or theoretical calculations (*21*, *22*). Commonly used experimental techniques are mass spectrometry and ion-mobility spectrometry (*23*, *24*). However, experimental methods require very complex instrumentation; thereby, the determination of experimental PAs is not often straightforward. Usually, theoretical calculations of PA and possible adduct complexes lead to absolute values.

Similarly, IE plays a crucial role in the selection of appropriate reagent ions to be used in the electron transfer reactions or adduct formation from NO^+ and O_2^+ reagent ions to the analyte molecule. If the IE of the analyte is less than the IE of NO (9.2 eV) and O_2 (12.2 eV) molecules, respectively, then electron transfer is favored in CI-MS from their respective ions. Similarly, if the IE of the analyte is comparable to NO, then adduct ions are formed. In a nutshell, PA and IE of the molecules determine the likelihood of a reaction followed by proton transfer or electron transfer from an appropriate reagent ion in the flow (drift) tubes.

The chemical reactivity of a molecular system which in turn is obtained from the global reactivity parameters is attributed to the HOMO and LUMO energy gap, as given by the Koopmann theorem (*25*). These quantities, for example, chemical potential (μ), chemical hardness (η), softness (ω), and electrophilic index (σ) are directly related to the properties and reactivity of the molecules (*26*, *27*). These reactivity descriptors provide a conceptual understanding of the relationship between structure, and stability, and are very effective in rationalizing the reactivity patterns of the molecular systems (*26*, *28*).

Recently, there has been much interest in the computational calculation of PA and IE values of the different classes of compounds (*29–32*). We report PAs and IEs of industrially important VOCs relevant to wine which include alcohols, esters, phenols, chloro and bromo-anisoles, and aldehydes (*3*, *33*). Presently, not much data on the PAs and IEs of the investigated compounds, either experimental or theoretical, are available. We provide a large database of the chemical properties of 45 VOCs useful in CI-MS quantification of undesirable trace gases in wine.

To find the suitability of the selected method, a benchmark study is conducted with popular density functional theory (DFT) functional, such as MP2 (Moller-Plesset with second-order energy correction), B_3LYP, and M06-2X (Minnesota 06). Only the indole molecule is evaluated, as none of the molecules have both PA and IE values reported in order to make comparisons. B_3LYP has been a gold standard DFT method, especially in the study of organic molecules, and is known to produce accurate ground state geometries and molecular properties at a reasonable computational cost. All initial structures were obtained from standard databases, such as PubChem and NIST (*34*, *35*). These structures are then geometrically relaxed to obtain the equilibrium geometry of the adopted DFT model. The minimized geometries were verified by calculating the vibrational energies to confirm there were no imaginary frequencies.

II Computational Method

State-of-the-art DFT calculations are carried out using the Gaussian '16' suite of software (*36*). The DFT method in conjunction with large and appropriate basis sets, which include polarization and diffuse functions, can produce reliable thermodynamic properties for molecular systems, including hydrogen bonding. The molecular geometry optimization is performed with B_3LYP (*37*) hybrid functional as a DFT method using 6-31+G(d, p) basis set comprising polarization and diffuse functions for heavy atoms. Polarization and diffuse functions greatly influence the reactivity parameters. PA of the VOCs is computed on fully optimized structures (neutral and protonated) in the gas phase as given below:

$$XH^+(g) + R(g) \longrightarrow RH^+(g) + X(g)\,. \tag{1}$$

is expressed as

$$PA = -\Delta E_{ele} - \Delta ZPE + \frac{5}{2}RT\,, \tag{2}$$

where ΔE_{ele} is the change in electronic energy to the protonated and neutral molecule. And, ΔZPE stands for the change in zero-point energy of normal mode in the protonated and neutral molecule. The last term in equation (2) represents the contribution from the translational energy of the proton. ΔE_{rot} contribution is zero since the proton doesn't have rotational kinetic energy. Similarly, ΔE_{vib} was neglected as compared to ΔZPE (usually less than 1 kcal/mol at room temperatures, i.e. less than experimental error).

Similarly, vertical/adiabatic ionization energies (VIEs/AIEs) of the VOCs are computed as the energy difference between an ionic and neutral state of the molecule. In VIEs, the energy of the optimized neutral structure is subtracted from the energy of the cation (or anion) at the optimized geometry of the neutral while in AIEs, energies of the optimized neutral structure are subtracted from the optimized cation (or anion) structure. In general, the IE is given as:

$$IE = E_0(N-1) - E_0(N)\,. \tag{3}$$

In addition, the atomic polar tensor (APT) (*28*) charge analysis is used to determine equivalent charges on the individual atoms from free bases and their protonated counterparts. The APT charges show modest basis set dependence and are sensitive to the correlation effects in the wave function, unlike Mulliken charge analysis which is basis set dependent, with the increased basis size, the actual charges may diverge significantly. The $\varepsilon_{HOMO-LUMO}$ energy gap together with the global reactivity parameters are computed using a similar level of DFT method as above. The choice of the B_3LYP/6-31+G(d, p) theory is consistent with the computational cost and required accuracy with the available experimental results.

We also computed PAs and IEs with MP2, B_3LYP, and M06-2X DFT functional for higher basis sets, such as 6-311+G(d, p), 6-311+G(3df, 2p), aug-cc-PVDZ, and aug-cc-PVTZ. The basis set 6-31+G(d, p) exhibits optimal experimental accuracy

as compared with the available PA and IE of indole molecule and is expected to perform better for the rest of the compounds occurring in the study.

III Results and Discussion

We open the discussion with Table 1 where PA and IE values are computed and listed for MP2, B_3LYP, and M06-2X DFT functional at several higher-level basis sets for indole molecule. MP2 provides slightly higher PAs, while M06-2X provides lower PAs than the reported experimental values for C4 attachment, see Fig. 1. B_3LYP/6-31+G(d, p) method appears to be in close agreement with the experimental PA and economical in terms of computational cost. It is observed that the protonation to N1 site provides far lesser PA than the experimental value of 216 kcal/mol, yet in compliance with previously computed B3LYP/6-31+G(d) results of 196.7 kcal/mol at N1 site (*38*). In general, the indole molecule contains seven preferred PA sites, out of which C4 appears to have higher PA in accordance with experimental value. Our computed PA at C4 site appears to be (214.49 kcal/mol) in excellent agreement with experimental and theoretical PAs (*38*, *39*).

Aug-cc-PVTZ basis set gives marginally better IE values, but lower PA than with 6-31+G(d, p) basis set, yet computationally expensive. The results obtained from 6-311+G(d, p), 6-311+G(3df, 2p), aug-cc-PVDZ, and aug-cc-PVTZ basis sets are almost identical, see Table 1. On the contrary, the MP2 method known to provide better electron correlation effects yields higher PAs and IEs than the experimental value. Similarly, M06-2X hybrid functional, which comprises 54% Hartree Fock (HF) exchange, follows MP2 IEs while PAs deviates from experimental results by a noticeable margin. B3LYP/6-31+G(d, p) has shown excellent results at a reasonable computational cost. Unfortunately, PA and IE data for other molecules were not available to make a fair comparison. Our computed results are thoroughly discussed below.

III.1 Proton Affinity

The PA values are obtained by using equation (2) and are reported in Table 2. The PA of the neutral molecule determines the preference of the reagent ion for CI-MS. A commonly used CI-MS technique, such as PTR-MS, typically employs H_3O^+ and NH_4^+ ions for the accurate quantification of trace gases. The proton transfer is exothermic and feasible when the PA of the analyte molecule is greater than the PA of the H_2O molecule. Likewise, protonation with NH_4^+ ions offer a great advantage, where H_3O^+ ions result in a high degree of fragmentation of certain functional groups, particularly alcohols, peroxides, esters, and other highly oxidized molecules. Proton transfer with NH_4^+ is generally more specific and occurs for molecules that possess higher PAs than NH_3, i.e, 204.5 kcal/mol (*19*).

In general, PA corresponds to the electronic redistribution and measures the stabilization experienced by the molecule after proton attachment. There will be a

rearrangement of the positions of the nuclei and electron density post-protonation. Notice that for a given molecule, the greater the negative charge on the atom, the more likely the proton attachment occurs. Our investigated molecules contain nitrogen, oxygen, chlorine, and bromine atoms with varying electronegativity values, which offer multiple active sites for protonation. The total energy of the selected molecules in neutral and protonated forms is computed and reported in Table 3. A full list of molecules with total energy, bond lengths, and APT charges is available in the supporting material.

We discuss fewer such molecules that contain more than one site for proton attachment. 2-sec-butyl-3-methoxypyrazine molecule shown in Fig. 2 offers oxygen and nitrogen as two potential protonation sites. Fig. 2 also represents a neutral molecule, Fig. 2a; protonated oxygen site, Fig. 2b; and protonated nitrogen site, Fig. 2c. We compute PA at both sites, corresponding to oxygen and nitrogen. PA at nitrogen is apparently higher (215.84 kcal/mol) as compared to the oxygen site (185.55 kcal/mol). Thereby, nitrogen on the pyrazine as shown in Fig. 2 is the preferred site for protonation. The high PA of a molecule indicates its higher propensity for a proton attachment.

Similarly, Fig. 3 represents the preferred site for protonation among two oxygen atoms where one of the oxygen sites has higher PA (site 3c with PA 191.50 kcal/mol). It is worth noting that, PA values are strongly affected by the different substituent groups (–CH_3, –OCH_3, –OC_2H_5, and –NH_2) attached to the carbonyl carbon. As seen in certain cases, for example, in Fig. 4, the water molecule gets separated from the carbonyl carbon atom of the octadien molecule when oxygen accepts a proton. In these circumstances, accommodation of a positive charge is much easier for the carbonyl carbon, as it is attached to the electron donor ethylene group in octadien molecule. Carbonyl carbon accommodates an additional positive charge (0.5416 au [neutral] to 0.7577 au [protonated]) consequently, C-O bond length increases from 1.43 Å to 1.62 Å and as a result, H_2O gets separated from the carbonyl carbon. Therefore, PA decreases when oxygen accepts a proton; it is so because bond breakage is an endothermic process. Due to this effect, lower PA values have been observed in some phenols, such as chloro and bromo phenols; and 2-chloro-6-methylphenol in comparison to other compounds. Nitrogen-containing molecules have the highest PA than other molecules.

In general, all the molecules under investigation can be protonated via nitrogen, oxygen, chlorine, and bromine active sites as the case might be. However, protonation to other sites makes the structure energetically unstable. For example, pentachloroanisole, 2,4,6-trichloroanisole, and 2,6-dichloroanisole do not show protonation to chlorine sites. Similarly, 2,4,6-tribromoanisole and pentabromophenol were unstable to proton attachment at bromine sites (see Table 3 for total energy values). While oxygen is the most favorable protonation site in all the above cases. From the reported PAs, rotundone (219.70 kcal/mol) was found to have the highest PA, while pentachlorophenol (167.15 kcal/mol) had the lowest PA. This means H_3O^+ can ionize pentachlorophenol and NH_4^+ is the best fit for rotundone's ionization through

effective proton transfer reactions.

Earlier reported data for PA (*40*) suggest that the oxygen-containing compounds found to have PA in the 180–205 kcal/mol range, and the nitrogen-containing compounds in the 205–240 kcal/mol range. Our computed values show excellent agreement to the above range, however inclusive data (experimental/theoretical) for the studied compounds will be imperative in the formal comparison.

III.2 Ionization Energy

In the selection of suitable reagent ion (gas) for electron transfer reactions using CI-MS ionization, prior knowledge of IE of the neutral molecule is needed. Electron transfer from commonly used ionizing ions in CI-MS, such as NO^+ and O_2^+ will be exothermic when an analytic molecule possesses less IE value than that of the corresponding reagent ion. NO^+ and O_2^+ ions are in particular of great advantage in CI-MS in separating isobars and isomers (*41–43*).

We compute IEs of various volatile compounds in gas-phase from equation (3). Both VIE and AIE are reported in column 4 of Table 2. The reported values show that the VIEs are more than the AIEs of the molecules. The available experimental value of IE in the case of the indole (7.76 eV) molecule coincides better with VIE (7.66 eV) rather than AIE (7.51 eV). Octanal has the highest IE value, while 1-methylindole having the lowest IE value among other molecules. The predicted IE trend shows that NO^+ can be used as a reagent ion for electron transfer except for the molecules, such as 2-methylisoborneol, octanal, 1-octene-3-one, and 1-octene-3-ol that possess higher IEs than NO molecule. VOCs namely, 2-methylisoborneol and 1-octene-3-one could lead to adduct formation as their IEs are comparable to NO. However, further experimental verification is needed to support this argument. Similarly, O_2^+ can ionize all the analyte molecules via dissociative charge transfer due to high IE of O_2 molecule and is preferred as an ionizing agent in gas-phase reactions where ionization with NO^+ is not possible.

One way to calculate the IE of a molecular system is by using equation (3). Another way to calculate IE is within the 'frozen molecular orbital' approximation given by the orbital energy as per the Koopmans theorem (*25*). In Koopmans approximation, originally applied in HF theory, if the orbitals of the system are unaffected by the loss of an electron then the vertical IE of an electron is given by the negative of the HOMO energy ($I_i \approx -\varepsilon_{\mathrm{HOMO}}$). However, implementing Kohn-Sham orbitals ($I_i \approx -\varepsilon_{\mathrm{highest,\ KS}}$) for the higher level of accuracy has been a subject of considerable analysis and discussion agreed by many authors (*44*, *45*) and concern for others (*46*, *47*).

In practice, it has been found that HF and typical Kohn–Sham procedures using hybrid functional produce valence orbital energies having magnitudes that tend to be larger and smaller respectively than the experimental IEs of the electrons as

$$|\varepsilon_{i,\mathrm{KS}}| < \mathrm{IE} < |\varepsilon_{\mathrm{i,HF}}|\,. \tag{4}$$

It is worth mentioning that our computed IE_i ($= -\varepsilon_{HOMO}$) as listed in Table 4 were lower by $\approx$ 1–2 eV than those obtained from equation (3) listed in Table 2. However, the reported theoretical results of $|\varepsilon_{i,\ KS}|$ deviate more than $|\varepsilon_{i,\ HF}|$ IEs, usually fall below 2–3 eV with BP86, B3PW91, and others (*48*). We have reported results using B_3LYP $\approx$ 1–2 eV deviation when compared with IE from Table 2. Interestingly, IE - IE_i difference is fairly uniform for all the valence orbitals in a molecule, suggesting that the error is somewhat systematic around 20% in the calculations.

III.3 Global Reactivity Parameters

PAs of the compounds discussed above cannot be utterly demonstrated by the local protonated site and carbonyl site only. Many protonation reactions in chemical ionization conditions may be under kinetic control, and the kinetically favored site of protonation might differ from the thermodynamically favored sites (*40*). Therefore, PA can not be fully interpreted by considering only the protonation of local sites, moreover, a contribution from overall molecular reactivity would be invaluable. The parameters of interest which determine the global reactivity of the molecule include electrophilic nature (ω), hardness (η), and softness (σ) can be obtained from the frontier molecular orbital energy gap ($\varepsilon_{HOMO-LUMO}$) of the targeted molecules. A lower $\varepsilon_{HOMO-LUMO}$ gap is crucial for eventual charge transfer within the molecule, however, a higher gap makes it difficult to add an electron to high-lying LUMO; to remove an electron from low-lying HOMO and therefore difficult to form the activated complex in any potential reaction. $\varepsilon_{HOMO-LUMO}$ energy diagram for indole molecule is shown in the supplementary material. Our reported energy gap (5.17 eV) perfectly allies with the NIST database value (5.17 eV) available for indole molecule. The chemical reactivity parameters are the response functions of the chemical system to the perturbation in its number of electrons (N), and external potential ($v(\vec{r})$). For example, electronic chemical potential (μ) is represented as the first derivative of energy w.r.t. the number of electrons (N). The chemical potential (μ) of a molecule is a measure of the electronegativity χ of the molecules ($\mu = -\chi$). Mathematically, global reactivity parameters are obtained as a function of ionization potential (I) and electron affinity (A).

$$\mu = \left(\frac{\partial \mathrm{E}}{\partial \mathrm{N}}\right)_{v(\vec{r})} \tag{5}$$

and

$$\eta = \left(\frac{\partial^2 \mathrm{E}}{\partial \mathrm{N}^2}\right)_{v(\vec{r})} = \left(\frac{\partial \mu}{\partial \mathrm{N}}\right)_{v(\vec{r})}. \tag{6}$$

Further, μ and η can be expressed in terms of ionization potential and electron affinity as

$$\mu = -\frac{1}{2}\,(\mathrm{I} + \mathrm{A}) \text{ and} \tag{7}$$

$$\eta = \frac{1}{2}\,(\mathrm{I} - \mathrm{A})\,. \tag{8}$$

Equations (7) and (8) are the energies of the frontier molecular orbitals ($\mathrm{I} \approx -\varepsilon_{\mathrm{HOMO}}$ and $\mathrm{A} \approx -\varepsilon_{\mathrm{LUMO}}$) according to the Koopmans theorem (*25*).

$$\mu = \frac{1}{2}\,(\varepsilon_{\mathrm{LUMO}} + \varepsilon_{\mathrm{HOMO}}) \text{ and} \tag{9}$$

$$\eta = \frac{1}{2}\,(\varepsilon_{\mathrm{LUMO}} - \varepsilon_{\mathrm{HOMO}})\,. \tag{10}$$

By following Koopmans approximation for closed-shell molecules, important chemical reactivity parameters can be obtained, namely, softness (σ) and electrophilic nature (ω) of the molecule as below:

$$\sigma = \frac{1}{2\eta}\,, \tag{11}$$

and electrophilic index (ω) of the molecule

$$\omega = \mu^2\sigma\,. \tag{12}$$

These parameters viz. chemical hardness (η), softness (σ), chemical potential (μ) and electrophilic index (ω) of the molecules as obtained from frontier molecular orbitals are listed in Table 4. The hardness (η) of a molecule represents its ground state stability and resistance to the system to exchange electronic charges with the environment. Hardness constitutes a valuable conception in understanding the behavior of chemical systems. Hard molecules have a large $\varepsilon_{\mathrm{HOMO-LUMO}}$ gap and possess high kinetic stability. While soft molecules, reciprocally, have a smaller $\varepsilon_{\mathrm{HOMO-LUMO}}$ gap and turned into low-stability compounds. Therefore, soft molecules can be easily polarized as compared to hard molecules. 2-methylisoborneol is highly stable and thus least reactive, with a high η (3.6177) value and a low σ value (0.1382) among other molecules. On the contrary, 2-aminoacetophenone with low η and corresponding a high σ value is highly reactive, having a low $\varepsilon_{\mathrm{HOMO-LUMO}}$ gap of 4.18 eV as compared to other molecules.

Chemical potential (μ) measures the tendency of an electron to escape from the equilibrium system. It is also associated with the electronegativity of a molecule. The larger the negative μ value, the higher will be the electronegativity of a molecule, and difficult for a system to lose an electron rather than easier to gain one. 4-ethylguaiacol (μ = -2.9469) is the least stable and highly reactive among the compounds. The electrophilic index ω of a molecule determines its molecular stability on receiving electron charge from the external environment. A high value of ω means a good electrophile while a lower one means a good nucleophile. Equation (12) refers to both the tendency to acquire more electronic charge μ^2 (square of the electronegativity) and the resistance of the system to exchange charge (η). In short, a good electrophile must have a high value of μ^2 and a low value of (η). From our reported data, we

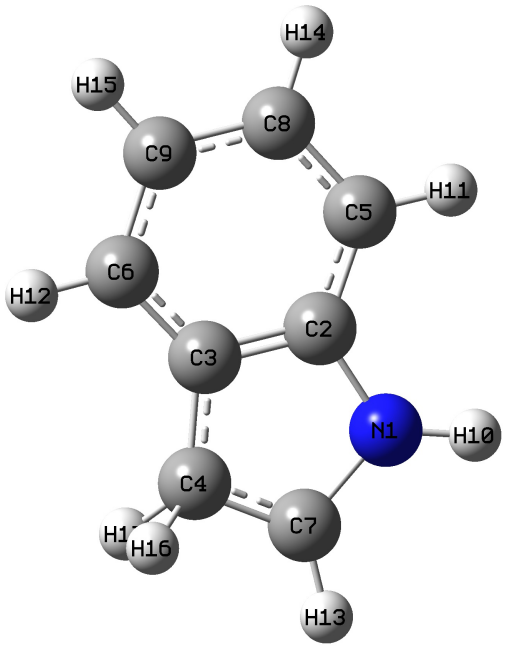

Figure 1: The indole molecule at kinetically preferred protonation site C4, with higher PA of 214.49 kcal/mol.

observe that pentabromophenol ($\omega = 4.6285$), 1-octen-3-one ($\omega = 3.9647$) and cis-1,5-octadien-3-one ($\omega = 3.9314$) are among the strong electrophiles. However, 4-ethylguaiacol is a good nucleophile. The computed global reactivity parameters are in eV, as indicated in Table 4.

IV Concluding Remarks

DFT calculations are used to compute PAs, IEs, and associated chemical properties, such as electrophilic nature (ω), chemical hardness (η), softness (σ), chemical potential (μ), and electronegativity (χ) of the VOCs linked to the taints and off-flavors in wine. A noteworthy quantitative approximation of the chemical properties can be obtained using a suitable combination of exchange and correlation functional. A benchmark analysis is carried out with popular DFT functional, such as MP2, B_3LYP, and M06-2X at higher basis set combinations. MP2 provides higher PAs and IEs than the experimental results, while M06-2X gives lower PAs and higher IEs, respectively. B_3LYP/6-31+G(d, p) appears par to be optimal in terms of computational cost and accuracy. Hybrid DFT functional B_3LYP with 6-31+G(d, p) basis set incorporating polarization and diffusion is applied for the evaluation of PA and IE values of the volatile compounds.

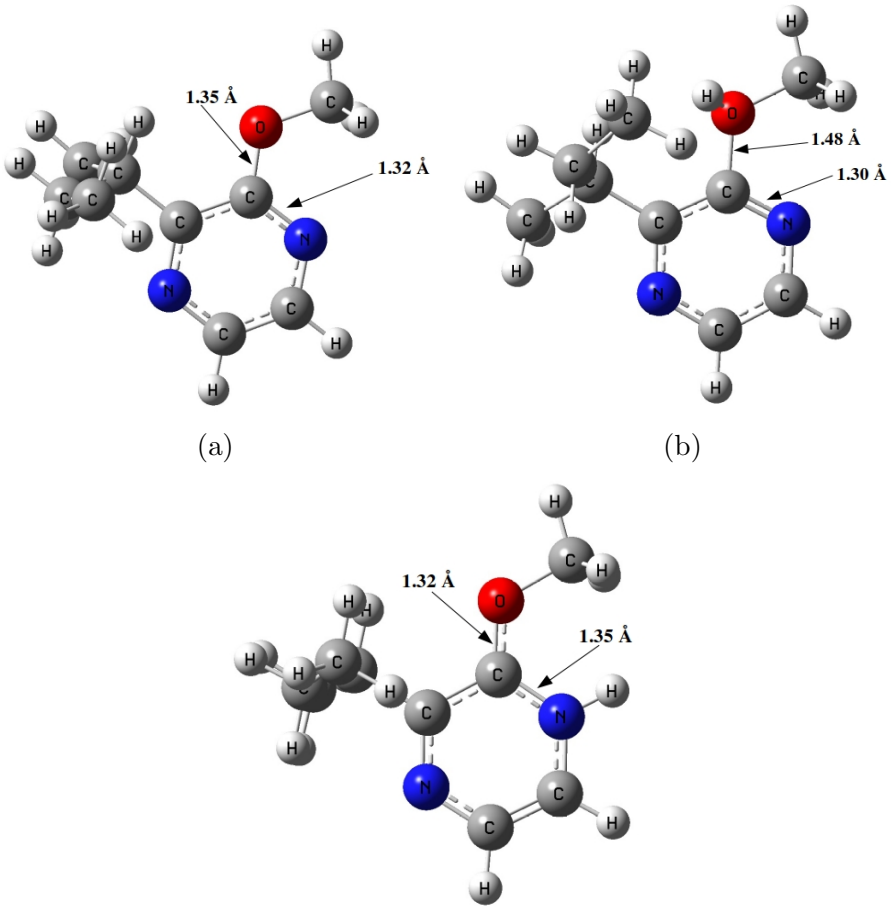

(a) (b)

(c)

Figure 2: Optimized structures of (2a) neutral, (2b) O-site protonated with PA 185.55 kcal/mol, (2c) N-site protonated, with PA 215.84 kcal/mol, 2-sec-butyl-3-methoxypyrazine molecule.

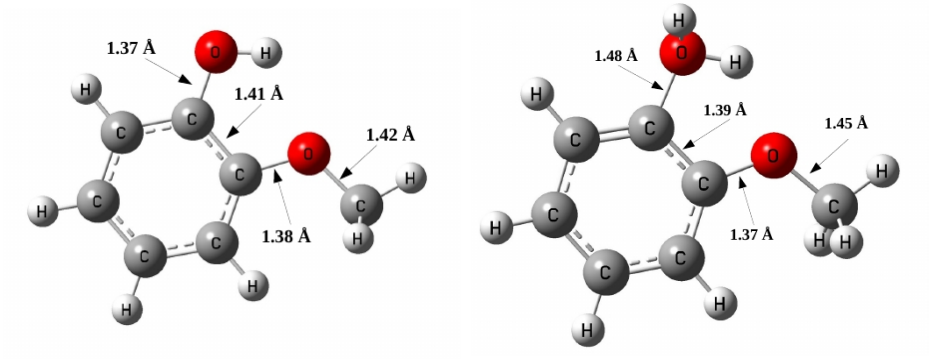

(a) (b)

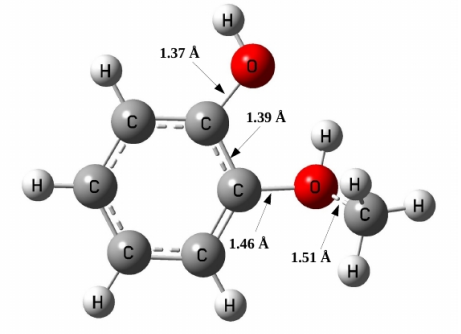

(c)

Figure 3: Optimized structures of (3a) neutral, (3b) HO-site protonated with PA 185.54 kcal/mol, (3c) CH_3-O-site protonated, with PA 191.50 kcal/mol, Guaiacol molecule.

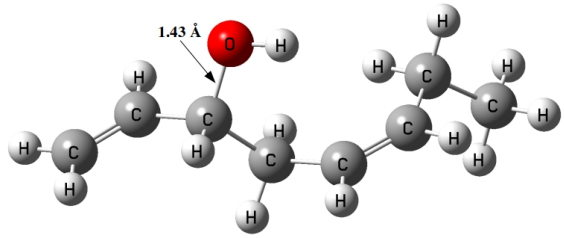

(a)

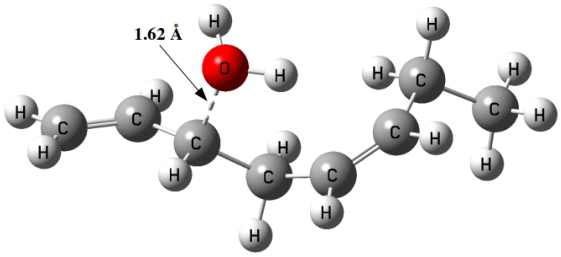

(b)

Figure 4: Fully optimized structures of (4a) neutral, and (4b) protonated, having PA 200.87 kcal/mol, cis-1,5-octadien-3-ol molecule to the oxygen site.

For PAs, both neutral and protonated structures are optimized to get the ground-state energies. The evaluated PA values are found to increase with the increasing carbon atom. The molecules comprising oxygen and nitrogen atoms are being preferred sites for proton attachment and found to have higher PAs, while chlorine and bromine do not show protonated complexes. Based on the PA values of VOCs, it is noted that H_3O^+ ions can effectively ionize lower PA molecules while NH_4^+ is suitable for higher PA molecules, for example, N-containing. Net APT charges and total energy of pre- and post-protonated species have also been computed to get a better understanding of the charge transfer process. A decrease in the net charge to the protonated site confirms that charge transfer from ligand to the added proton has been taken place.

The computed VIEs seem to have a close rationale with experimental results, as available, e.g. indole molecule. The predicted VIE values are higher than that of AIE values. IE values show that NO^+ can be used to ionize analyte molecules with some exceptions where molecules possess higher IEs than NO molecule, while O_2^+ can ionize all the analyte molecules as predicted based on IE values. The global reactivity parameters further strengthen the knowledge of the overall chemical reactivity and electrophilic nature of a reactant molecule in a reaction, useful for rationalizing trends without having to perform time-consuming calculations.

These reactivity parameters along with PA and IE data are the major ingredients in understanding the reaction kinetics of VOCs with reagent ions in CI-MS quantification. The computed molecular properties will be helpful in the identification

and quantification of trace gases using CI-MS techniques. In particular, PA and IE values will serve as the principal quantities in the selection of appropriate reagent gas (ions) in CI-MS using PTR-MS/SIFT-MS analytic techniques.

Acknowledgments. Computational resources from CINECA are greatly appreciated. Financial support from Fondazione Edmund Mach (ADP, 2018) is acknowledged.

Supporting Material: Data on the total energy at the stationary point of the neutral and protonated complex together with the net atomic charge, bond length change post protonation are collected as supplementary material for all species occurring in this study.

References

(*1*) Waterhouse, A., Sacks, G., and Jeffery, D. In *Understanding Wine Chemistry*; John Wiley & Sons: 2016, pp 16–25.

(*2*) Tarasov, A., Rauhut, D., and Jung, R. (2017). Cork taint responsible compounds. Determination of haloanisoles and halophenols in cork matrix: A review. *Talanta 175*, 82–92.

(*3*) Bianco, G., Novario, G., Zianni, R., and Cataldi, T. R. I. (2009). Comparison of two SPME fibers for the extraction of some off-flavor cork-taint compounds in bottled wines investigated by GC-HRMS. *Anal. Bioanal. Chem. 393*, 2019–2027.

(*4*) Pereira, C. S., Marques, J. J. F., and Romão, M. V. S. (2010). Cork Taint in Wine: Scientific Knowledge and Public Perception-A Critical Review. *Crit. Rev. Microbiol. 26*, 147–162.

(*5*) Sefton, M. A., and Simpson, R. F. (2005). Compounds causing cork taint and the factors affecting their transfer from natural cork closures to wine – a review. *Aus. J. Grape Wine Res. 11*, 226–240.

(*6*) Scott, E. S., Dambergs, R., and Stummer, B. In *Managing Wine Quality*, Reynolds, A. G., Ed.; Woodhead Publishing Limited, Cambridge, United Kingdom: 2010, pp 481–514.

(*7*) S., V., García-Vallejo, M., Cadahía, E., and Fernández de Simón, B. (2001). Polyphenols susceptible to migrate from cork stoppers to wine. *Eur. Food Res. Technol. 213*, 56–61.

(*8*) Riu, M., Mestres, M., Busto, O., and Guasch, J. (2007). Comparative study of two chromatographic methods for quantifying 2,4,6-trichloranisole in wines. *J. Chromatogr. A 1138*, 18–25.

(*9*) Butzke, C. E., Evans, T. J., and Ebeler, S. E. In *Chemistry of Wine Flavor*; American Chemical Society: US, 1998; Vol. 714; Chapter 15, pp 208–216.

(*10*) Ridgway, K., Lalljie, S. P. D., and Smith, R. M. (2010). Analysis of food taints and off-flavours: a review. *Food Addit. Contam. 27*, 146–168.

(*11*) Romano, A., Fischer, L., Herbig, J., Campbell-Sills, H., Coulon, J., Lucas, P., Cappellin, L., and Biasioli, F. (2014). Wine analysis by FastGC proton-transfer reaction-time-of-flight-mass spectrometry. *Int. J. Mass Spectrom. 369*, 81–86.

(*12*) Boscaini, E., Mikoviny, T., Wisthaler, A., von Hartungen, E., and Märk, T. D. (2004). Characterization of wine with PTR-MS. *Int. J. Mass Spectrom. 239*, 215–219.

(*13*) Hansel, A., Jordan, A., Holzinger, R., Prazeller, P., Vogel, W., and Lindinger, W. (1995). Proton transfer reaction mass spectrometry: on-line trace gas analysis at the ppb level. *Int. J. Mass Spectrom. Ion Process. 149-150*, 609–619.

(*14*) Španěl, P., and Smith, D. (1996). Selected ion flow tube: a technique for quantitative trace gas analysis of air and breath. *Med. Biol. Eng. Comput. 34*, 409–419.

(*15*) Cappellin, L., Karl, T., Probst, M., Ismailova, O., Winkler, P., Soukoulis, C., Aprea, E., Märk, T., Gasperi, F., and Biasioli, F. (2012). On Quantitative Determination of Volatile Organic Compound Concentrations Using Proton Transfer Reaction Time-of-Flight Mass Spectrometry. *Environ. Sci. Technol. 46*, 2283–2290.

(*16*) Ellis, A., and Mayhew, C. In *Proton Transfer Reaction Mass Spectrometry*; John Wiley & Sons, Ltd: 2013; Chapter 4, pp 111–127.

(*17*) Ellis, A., and Mayhew, C. In *Proton Transfer Reaction Mass Spectrometry*; John Wiley & Sons, Ltd: 2014; Chapter 2, pp 25–48.

(*18*) Fujii, T. In *Ion/Molecule Attachment Reactions: Mass Spectrometry*; Springer US: 2015, pp 263–302.

(*19*) Ellis, A. M., and Mayhew, C. A. In *Proton Transfer Reaction Mass Spectrometry Principles and Applications*, 1st ed.; John Wiley & Sons: UK, 2014; Chapter 2, p 38.

(*20*) Canaval, E., Hyttinen, N., Schmidbauer, B., Fischer, L., and Hansel, A. (2019). NH_4^+ Association and Proton Transfer Reactions With a Series of Organic Molecules. *Front. Chem. 7*, 191–206.

(*21*) Koppel, I. A., Taft, R. W., Anvia, F., Zhu, S.-Z., Hu, L.-Q., Sung, K.-S., DesMarteau, D. D., Yagupolskii, L. M., and Yagupolskii, Y. L. a. (1994). The Gas-Phase Acidities of Very Strong Neutral Bronsted Acids. *J. Am. Chem. Soc. 116*, 3047–3057.

(*22*) Ligon, A. P. (2000). Theoretical Calculations of the Proton Affinities ofn-Alkylamines,n-Alkyl Thiols, andn-Alcohols and the Ammonium Affinities of then-Alcohols. *J. Phys. Chem. A 104*, 8739–8743.

(*23*) da Silva, E. F. (2005). Comparison of Quantum Mechanical and Experimental Gas-Phase Basicities of Amines and Alcohols. *J. Phys. Chem. A 109*, 1603–1607.

(*24*) Tabrizchi, M., and Shooshtari, S. (2003). Proton affinity measurements using ion mobility spectrometry. *J. Chem. Thermodyn. 35*, 863–870.

(*25*) Koopmans, T. (1934). Ordering of wave functions and eigenvalues to the individual electrons of an atom. *Physica 1*, 104–110.

(*26*) Maity, R., Mandal, D., and Misra, A. (2020). Role of Π-electron conjugation in determining the electrical responsive properties of polychlorinated biphenyls: a DFT based computational study. *SN Appl. Sci. 2*, 1–11.

(*27*) Flores, N., Frau, J., and Glossman-Mitnik, D. (2019). Chemical-Reactivity Properties, Drug Likeness, and Bioactivity Scores of Seragamides A–F Anticancer Marine Peptides: Conceptual Density Functional Theory Viewpoint. *Computation 7*, 52.

(*28*) Jensen, F. In *Introduction to Computational Chemistry*; Wiley: 2017.

(*29*) Wróblewski, T., Ziemczonek, L., Alhasan, A. M., and Karwasz, G. (2007). Ab initio and density functional theory calculations of proton affinities for volatile organic compounds. *Eur. Phys. J. Spec. Top. 144*, 191–195.

(*30*) Chandra, A. K., and Goursot, A. (1996). Calculation of Proton Affinities Using Density Functional Procedures: A Critical Study. *J. Phys. Chem. 100*, 11596–11599.

(*31*) Valadbeigi, Y., Farrokhpour, H., and Tabrizchi, M. (2014). G4MP2, DFT and CBS-Q calculation of proton and electron affinities, gas phase basicities and ionization energies of hydroxylamines and alkanolamines. *J. Chem. Sci. 126*, 1209–1215.

(*32*) Ghahremani, M., Bahrami, H., Douroudgari, H., and Vahedpour, M. (2020). Theoretical prediction of proton and electron affinities, gas phase basicities, and ionization energies of sulfinamides. *Struct. Chem. 31*, 411–421.

(*33*) Özhan, D., Anli, R. E., Vural, N., and Bayram, M. (2012). Determination of Chloroanisoles and Chlorophenols in Cork and Wine by using HS-SPME and GC-ECD Detection. *J. Inst. Brew. 115*, 71–7.

(*34*) PubChem data-base, https://pubchem.ncbi.nlm.nih.gov/, Accessed: 2020-05-30.

(*35*) NIST data-base, https://webbook.nist.gov/chemistry/, Accessed: 2020-05-30.

(*36*) Frisch, M. J., Trucks, G. W., Schlegel, H. B., Scuseria, G. E., Robb, M. A., Cheeseman, J. R., Scalmani, G., Barone, V., Petersson, G. A., Nakatsuji, H., Li, X., Caricato, M., Marenich, A. V., Bloino, J., Janesko, B. G., Gomperts, R., Mennucci, B., Hratchian, H. P., Ortiz, J. V., Izmaylov, A. F., Sonnenberg, J. L., Williams-Young, D., Ding, F., Lipparini, F., Egidi, F., Goings, J., Peng, B., Petrone, A., Henderson, T., Ranasinghe, D., Zakrzewski, V. G., Gao, J., Rega, N., Zheng, G., Liang, W., Hada, M., Ehara, M., Toyota, K., Fukuda, R., Hasegawa, J., Ishida, M., Nakajima, T., Honda, Y., Kitao, O., Nakai, H., Vreven, T., Throssell, K., Montgomery, J. A., Jr., Peralta, J. E., Ogliaro, F., Bearpark, M. J., Heyd, J. J., Brothers, E. N., Kudin, K. N., Staroverov, V. N., Keith, T. A., Kobayashi, R., Normand, J., Raghavachari, K., Rendell, A. P., Burant, J. C., Iyengar, S. S., Tomasi, J., Cossi, M., Millam, J. M., Klene, M., Adamo, C., Cammi, R., Ochterski, J. W., Martin, R. L., Morokuma, K., Farkas, O., Foresman, J. B., and Fox, D. J. Gaussian˜16 Revision C.01, Gaussian Inc. Wallingford CT, 2016.

(*37*) Lee, C., Yang, W., and Parr, R. G. (1988). Development of the Colle-Salvetti correlation-energy formula into a functional of the electron density. *Phys. Rev. B 37*, 785–789.

(*38*) Charmet, A. P., Quartarone, G., Ronchin, L., Tortato, C., and Vavasori, A. (2013). Quantum Chemical Investigation on Indole: Vibrational Force Field and Theoretical Determination of Its Aqueous pKa Value. *J. Phys. Chem. A 117*, PMID: 23899419, 6846–6858.

(*39*) Somers, K., Kryachko, E., and Ceulemans, A. (2004). Theoretical study of indole: Protonation, indolyl radical, tautomers of indole, and its interaction with water. *Chem. Phys. 301*, 61–79.

(*40*) Harrison, A. G. In *Chemical Ionization Mass Spectrometry*, 2nd ed.; Taylor & Francis: Canada, 1992; Chapter 2, pp 7–41.

(*41*) Castada, H. Z., Barringer, S. A., and Wick, M. (2017). Gas-phase chemical ionization of 4-alkyl branched-chain carboxylic acids and 3-methylindole using H_3O^+, NO^+ and O_2^+ ions. *Rapid Commun. Mass Spectrom. 31*, 1641–1650.

(*42*) Wang, T., Spanel, P., and Smith, D. (2003). Selected Ion Flow Tube, SIFT, studies of the reactions of H_3O^+, NO^+ and O_2^+ with eleven $C_{10}H_{16}$ monoterpenes. *Int. J. Mass Spectrom. 228*, 117–126.

(*43*) Španěl, P., Wang, T., and Smith, D. (2002). A selected ion flow tube, SIFT, study of the reactions of H_3O^+, NO^+ and O_2^+ ions with a series of diols. *Int. J. Mass Spectrom. 218*, 227–236.

(*44*) Kleinman, L. (1997). Significance of the highest occupied Kohn-Sham eigenvalue. *Phys. Rev. B 56*, 12042–12045.

(*45*) Harbola, M. K. (1999). Relationship between the highest occupied Kohn-Sham orbital eigenvalue and ionization energy. *Phys. Rev. B 60*, 4545–4550.

(*46*) Chong, D. P., Gritsenko, O. V., and Baerends, E. J. (2002). Interpretation of the Kohn–Sham orbital energies as approximate vertical ionization potentials. *J. Chem. Phys. 116*, 1760–1772.

(*47*) Gritsenko, O. V., Braïda, B., and Baerends, E. J. (2003). Physical interpretation and evaluation of the Kohn–Sham and Dyson components of the ϵ-I relations between the Kohn–Sham orbital energies and the ionization potentials. *J. Chem. Phys. 119*, 1937–1950.

(*48*) Politzer, P., and Murray, J. S. In *Theoretical Aspects of Chemical Reactivity*, Toro-Labbé, A., Ed.; Theoretical and Computational Chemistry, Vol. 19; Elsevier: 2007, pp 119–137.

(*49*) Lias, S., Bartmess, J., Liebman, J., Holmes, J., Levin, R., and Mallard, W. In *Gas-phase ion and neutral thermochemistry*; Journal of Physical and Chemic; American Chemical Society and the American Institute of Physics: 1988.

Table 1: Evaluation of MP2, B_3LYP, and M06-2X proton affinity (PA) values at N1 and C4 protonation sites; in kcal/mol, and ionization energy (IE); in eV, of Indole* molecule against different basis sets.

Basis Set	**MP2**		**B_3LYP**		**M06-2X**	
	PA	IE	PA	IE	PA	IE
6-31+G(d, p)	197.33 (N1)	8.60	199.49 (N1)	7.66	196.78 (N1)	7.96
	220.72 (C4)		214.49 (C4)		210.26 (C4)	
6-311+G(d, p)	195.74 (N1)	8.75	199.01 (N1)	7.72	196.39 (N1)	8.02
	220.93 (C4)		212.64 (C4)		209.51 (C4)	
6-311+G(3df, 2p)	194.00 (N1)	8.89	198.73 (N1)	7.72	196.22 (N1)	8.03
	220.82 (C4)		213.42 (C4)		209.37 (C4)	
Aug-cc-PVDZ	194.98 (N1)	8.85	198.68 (N1)	7.69	196.51 (N1)	7.96
	220.97 (C4)		213.54 (C4)		209.91 (C4)	
Aug-cc-PVTZ	194.91 (N1)	8.93	199.32 (N1)	7.72	196.52 (N1)	8.02
	220.83 (C4)		213.69 (C4)		209.83 (C4)	

* Experimental values of PA and IE for indole are 216 kcal/mol and 7.76 eV, respectively (*49*). Protonation at C4 site with B_3LYP/6-31+G(d, p) is in excellent agreement with the experimental and theoretical results (*39*).

Table 2: Computed values of proton affinity (PA), vertical ionization energy and adiabatic ionization energy (in brackets) of VOCs responsible for taints and off-flavors in wine and food.

Molecule name	**CAS number**	**PA** kcal/mol	**VIE (AIE)** eV
2,4,6-Trichloroanisole ($C_7H_5Cl_3O$)	87-40-1	183.51	8.87 [8.28]
2,4,6-Tribromoanisole ($C_7H_5Br_3O$)	607-99-8	186.17	8.67 [8.19]
Pentachlorophenol (C_6Cl_5OH)	87-86-5	167.15	8.76 [8.56]
Pentabromophenol (C_6Br_5OH)	608-71-9	174.17	8.75 [8.60]
2,4,6-Trichlorophenol ($C_6H_2Cl_3OH$)	88-06-2	174.35	9.03 [8.79]
2,4,6-Tribromophenol ($C_6H_2Br_3OH$)	118-79-6	178.56	8.81 [8.62]
2,3,4-Trichloroanisole ($C_7H_5Cl_3O$)	54135-80-7	181.32	8.36 [8.15]
2,3,6-Trichloroanisole ($C_7H_5Cl_3O$)	50375-10-5	183.87	8.83 [8.37]
2,3,4,5-Tetrachloroanisole ($C_7H_4Cl_4O$)	938-86-3	178.40	8.44 [8.23]
2,3,4,6-Tetrachloroanisole ($C_7H_4Cl_4O$)	938-22-7	181.96	8.85 [8.35]
2,3,5,6-Tetrachloroanisole ($C_7H_4Cl_4O$)	6936-40-9	181.49	8.85 [8.67]
2,4-Dichloroanisole ($C_7H_6Cl_2O$)	553-82-2	182.77	8.26 [8.04]
2,6-Dichloroanisole ($C_7H_6Cl_2O$)	1984-65-2	186.69	8.96 [8.30]
Cis-1,5-octadien-3-one ($C_8H_{12}O$)	65767-22-8	211.13	8.70 [8.39]
Cis-1,5-octadien-3-ol ($C_8H_{14}O$)	50306-18-8	200.87	8.72 [8.28]
1-Octene-3-ol ($C_8H_{16}O$)	3391-86-4	197.68	9.37 [8.92]
1-Octene-3-one ($C_8H_{14}O$)	4312-99-6	203.94	9.23 [9.01]
Octanal ($C_8H_{16}O$)	124-13-0	192.82	9.38 [9.18]
2-Sec-butyl-3-methoxypyrazine ($C_9H_{14}N_2O$)	24168-70-5	215.84	8.53 [8.30]
3-Iso-butyl-2-methoxypyrazine ($C_9H_{14}N_2O$)	24683-00-9	215.77	8.51 [8.28]
2-Iso-propyl-3-methoxypyrazine ($C_8H_{12}N_2O$)	25773-40-4	215.39	8.56 [8.33]
2-Methoxy-3,5-dimethylpyrazine ($C_9H_{10}N_2O$)	92508-08-2	217.16	8.32 [8.11]

Table 2: continues

Molecule name	**CAS number**	**PA** kcal/mol	**VIE (AIE)** eV
2-Methylisoborneol ($C_{11}H_{20}O$)	2371-42-8	217.79	9.21 [8.28]
Geosmin ($C_{12}H_{22}O$)	19700-21-1	205.05	8.86 [8.35]
Guaiacol ($C_7H_8O_2$)	90-05-1	191.50	7.91 [7.66]
4-Ethylguaiacol ($C_9H_{12}O_2$)	2785-89-9	198.28	7.55 [7.29]
4-Ethylphenol ($C_8H_{10}O$)	123-07-9	182.32	8.07 [7.86]
Eucalyptol ($C_8H_{10}O$)	470-82-6	213.24	8.46 [8.28]
4-Ethylcatechol ($C_8H_{10}O_2$)	1124-39-6	198.28	7.85 [7.61]
4-Methylguaiacol ($C_8H_{10}O_2$)	93-51-6	195.18	7.58 [7.32]
Rotundone ($C_{15}H_{22}O$)	18374-76-0	219.70	8.36 [8.18]
Geraniol ($C_{10}H_{18}O$)	106-24-1	212.37	8.10 [7.77]
Hotrienol ($C_{10}H_{16}O$)	53834-70-1	208.05	7.99 [7.73]
Linalool ($C_{10}H_{18}O$)	78-70-6	214.27	8.38 [8.03]
Nerol ($C_{10}H_{18}O$)	106-25-2	209.87	8.37 [7.91]
$\alpha-$Terpineol ($C_{10}H_{18}O$)	98-55-5	200.56	8.23 [7.95]
Indole (C_8H_7N)	120-72-9	214.49	7.66 [7.51]
1-Methylindole (C_9H_9N)	603-76-9	203.64	7.44 [7.30]
2-Aminoacetophenone (C_8H_9NO)	551-93-9	214.57	7.74 [7.61]
2-Chloro-6-methylphenol (C_7H_7ClO)	87-64-9	177.47	8.41 [8.20]
3-Octanone ($C_8H_{16}O$)	106-68-3	203.37	9.12 [8.92]
Fenchone ($C_{10}H_{16}O$)	1195-79-5	207.11	8.55 [8.33]
Fenchol ($C_{10}H_{18}O$)	1632-73-1	198.48	9.15 [8.31]
Trans-2-octen-1-ol ($C_8H_{16}O$)	18409-17-1	203.08	8.94 [8.53]
Pentachloroanisole ($C_7H_3Cl_5O$)	1825-21-4	180.35	8.95 [8.44]

Table 3: Net charge (au) on the atoms before and after protonation (in square brackets) is represented for selected molecules, along with their corresponding total energies (au).

Molecule name	**Net atomic charge**	**Total Energy**
2,4,6-Trichloroanisole	O–H^+[-0.7929, -0.5878]	-1725.8685
($C_7H_5Cl_3O$)	Cl(2[1])–H^+[-0.2964, 0.0701]	-1725.8161
2,4,6-Tribromoanisole	O–H^+ [-0.7859, -0.6063]	-8060.4741
($C_7H_5Br_3O$)	Br(2)–H^+ [-0.2101, -0.1283]	-8060.4314
Pentabromophenol	O–H^+[-0.6943, -0.6846]	-13163.3932
(C_6Br_5OH)	Br(2)–H^+[-0.1647, 0.4083]	-13163.3541
2,3,4-Trichloroanisole	O–H^+[-0.8974, -0.8248]	-1725.8617
($C_7H_5Cl_3O$)	Cl(1)–H^+[-0.2408, -0.0479]	-1725.8282
2-Sec-butyl-3-	N–H^+[-0.3568, -0.1456]	-536.5060
methoxypyrazine	CH_3O–H^+[-0.8789, -0.7715]	-536.4563
($C_9H_{14}N_2O$)		
3-Iso-butyl-2-	N–H^+[-0.3515, -0.1428]	-536.5046
methoxypyrazine	CH_3O–H^+[-0.8736, -0.7837]	-536.4538
($C_9H_{14}N_2O$)		
2-Iso-propyl-3-	N–H^+[-0.3606, -0.1505]	-497.1885
methoxypyrazine	CH_3O–H^+[-0.8878, -0.7556]	-497.1360
($C_8H_{12}N_2O$)		
2-Methoxy-3,5-	N–H^+[-0.3462, -0.1293]	-457.8814
dimethylpyrazine	O–H^+[-0.9178, -0.6658]	-457.8298
($C_9H_{10}N_2O$)		
Guaiacol	CH_3O–H^+[-0.8829, -0.6341]	-422.3394
($C_7H_8O_2$)	HO–H^+[-0.7178, -0.5607]	-422.3297
4-Ethylguaiacol	CH_3O–H^+[-0.8697, -0.6441]	-500.9803
($C_9H_{12}O_2$)	HO–H^+[-0.7108, -0.4470]	-500.9702
4-Methylguaiacol	CH_3O–H^+[-0.8704, -0.6391]	-461.6627
($C_8H_{10}O_2$)	HO–H^+[-0.7001, -0.5711]	-461.6536
2-Aminoacetophenone	O–H^+[-0.7814, -0.7688]	-440.6478
(C_8H_9NO)	H_2N–H^+[-0.7450, -0.2077]	-440.6437
Pentachloroanisole	CH_3O–H^+[-0.8200, -0.6120]	-2645.0284
($C_7H_3Cl_5O$)	Cl(2)–H^+[0.2335, -0.0293]	-2644.9842

[1]Position of the atom in a molecule.

Table 4: Computed chemical reactivity parameters: energy of frontier molecular orbitals ($\varepsilon_{\mathrm{HOMO}}$, $\varepsilon_{\mathrm{LUMO}}$), hardness ($\eta$), softness ($\sigma$), chemical potential ($\mu$), and electrophilic index (ω) of VOCs in gas phase. (Note: all quantities are in eV; $\varepsilon_{\mathrm{HOMO}}$, $\varepsilon_{\mathrm{LUMO}}$ and μ are referred to the vacuum energy far from the molecule).

Molecule name	$\boldsymbol{\varepsilon_{\mathrm{HOMO}}}$	$\boldsymbol{\varepsilon_{\mathrm{LUMO}}}$	$\boldsymbol{\eta}$	$\boldsymbol{\sigma}$	$\boldsymbol{\mu}$	$\boldsymbol{\omega}$
2,4,6-Trichloroanisole ($C_7H_5Cl_3O$)	-7.0994	-1.3660	2.8667	0.1747	-4.2327	3.1248
2,4,6-Tribromoanisole ($C_7H_5Br_3O$)	-6.9906	-1.4013	2.7946	0.1789	-4.1959	3.1500
Pentachlorophenol (C_6Cl_5OH)	-7.3715	-1.7741	2.7986	0.1786	-4.5728	3.7358
Pentabromophenol (C_6Br_5OH)	-7.1647	-2.3129	2.4258	0.2061	-4.7388	4.6285
2,4,6-Trichlorophenol ($C_6H_2Cl_3OH$)	-7.1620	-1.3306	2.9157	0.1714	-4.2463	3.0921
2,4,6-Tribromophenol ($C_6H_2Br_3OH$)	-7.0668	-1.4422	2.8122	0.1777	-4.2545	3.2181
2,3,4-Trichloroanisole ($C_7H_5Cl_3O$)	-6.6042	-1.1836	2.7102	0.1844	-3.8939	2.7973
2,3,6-Trichloroanisole ($C_7H_5Cl_3O$)	-7.0450	-1.1836	2.9306	0.1706	-4.1143	2.8880
2,3,4,5-Tetrachloroanisole ($C_7H_4Cl_4O$)	-6.7783	-1.3687	2.7048	0.1848	-4.0735	3.0674
2,3,4,6-Tetrachloroanisole ($C_7H_4Cl_4O$)	-7.1321	-1.5075	2.8122	0.1777	-4.3198	3.3177
2,3,5,6-Tetrachloroanisole ($C_7H_4Cl_4O$)	-7.1348	-1.4340	2.8503	0.1754	-4.2844	3.2199
2,4-Dichloroanisole ($C_7H_6Cl_2O$)	-6.4354	-1.0394	2.6980	0.1853	-3.7374	2.5887
2,6-Dichloroanisole ($C_7H_6Cl_2O$)	-7.0967	-0.9877	3.0544	0.1636	-4.0422	2.6747
Cis-1,5-octadien-3-one ($C_8H_{12}O$)	-6.7674	-1.9428	2.4122	0.2072	-4.3551	3.9314
Cis-1,5-octadien-3-ol ($C_8H_{14}O$)	-6.9144	-0.3646	3.2748	0.1526	-3.6395	2.0223
1-Octene-3-ol ($C_8H_{16}O$)	-7.3443	-0.3918	3.4762	0.1438	-3.8681	2.1520
1-Octene-3-one ($C_8H_{14}O$)	-7.0640	-1.9456	2.5592	0.1953	-4.5048	3.9647
Octanal ($C_8H_{16}O$)	-7.1321	-1.0748	3.0286	0.1650	-4.1034	2.7798
2-Sec-butyl-3-methoxypyrazine ($C_9H_{14}N_2O$)	-6.6395	-1.3986	2.6204	0.1908	-4.0191	3.0821
3-Iso-butyl-2-methoxypyrazine($C_9H_{14}N_2O$)	-6.6314	-1.4095	2.6109	0.1915	-4.0204	3.0955
2-Iso-propyl-3-methoxypyrazine ($C_8H_{12}N_2O$	-6.6423	-1.4068	2.6177	0.1910	-4.0245	3.0937
2-Methoxy-3,5-dimethylpyrazine($C_9H_{10}N_2O$)	-6.4028	-1.2353	2.5837	0.1935	-3.8191	2.8226

Table 4: continued

Molecule name	$\varepsilon_{\mathrm{HOMO}}$	$\varepsilon_{\mathrm{LUMO}}$	η	σ	μ	ω
2-Methylisoborneol ($C_{11}H_{20}O$)	-7.2844	-0.0489	3.6177	0.1382	-3.6667	1.8581
Geosmin ($C_{12}H_{22}O$)	-7.0804	-0.1360	3.4721	0.1440	-3.6082	1.8748
Guaiacol ($C_7H_8O_2$)	-5.9048	-0.2149	2.8449	0.1757	-3.0599	1.6455
4-Ethylguaiacol ($C_9H_{12}O_2$)	-5.6735	-0.2204	2.7265	0.1833	-2.9469	1.5926
4-Ethylphenol ($C_8H_{10}O$)	-6.0871	-0.4489	2.8191	0.1773	-3.2680	1.8942
Eucalyptol ($C_8H_{10}O$)	-6.5171	-0.0408	3.2381	0.1544	-3.2789	1.6601
4-Ethylcatechol ($C_8H_{10}O_2$)	-5.8939	-0.3836	2.7551	0.1814	-3.1388	1.7879
4-Methylguaiacol ($C_8H_{10}O_2$)	-5.6762	-0.2340	2.7211	0.1837	-2.9551	1.6046
Rotundone ($C_{15}H_{22}O$)	-6.6259	-1.3605	2.6327	0.1899	-3.9932	3.0284
Geraniol ($C_{10}H_{18}O$)	-6.4082	-0.2857	3.0612	0.1633	-3.3470	1.8296
Hotrienol ($C_{10}H_{16}O$)	-6.0953	-0.8136	2.6408	0.1893	-3.4544	2.2593
Linalool ($C_{10}H_{18}O$)	-6.4463	-0.2857	3.0803	0.1623	-3.3660	1.8391
Nerol ($C_{10}H_{18}O$)	-6.6423	-0.2204	3.2109	0.1557	-3.4313	1.8334
$\alpha-$Terpineol ($C_{10}H_{18}O$)	-6.2096	-0.1795	3.0150	0.1658	-3.1946	1.6924
Indole (C_8H_7N)	-5.7388	-0.5659	2.5864	0.1933	-3.1524	1.9211
1-Methylindole (C_9H_9N)	-5.6001	-0.5523	2.5238	0.1981	-3.0762	1.8747
2-Aminoacetophenone (C_8H_9NO)	-5.8395	-1.6598	2.0898	0.2392	-3.7497	3.3640
2-Chloro-6-methylphenol(C_7H_7ClO)	-6.4436	-0.6449	2.8993	0.1724	-3.5442	2.1663
3-Octanone ($C_8H_{16}O$)	-6.8790	-0.6013	3.1388	0.1592	-3.7402	2.2283
Fenchone ($C_{10}H_{16}O$)	-6.5008	-0.6340	2.9333	0.1704	-3.5674	2.1692
Fenchol ($C_{10}H_{18}O$)	-7.1729	-0.1115	3.5306	0.1416	-3.6422	1.8786
Trans-2-octen-1-ol ($C_8H_{16}O$)	-6.8844	-0.2966	3.2939	0.1517	-3.5905	1.9569
Pentachloroanisole ($C_7H_3Cl_5O$)	-7.2600	-1.6517	2.8041	0.1783	-4.4558	3.5402

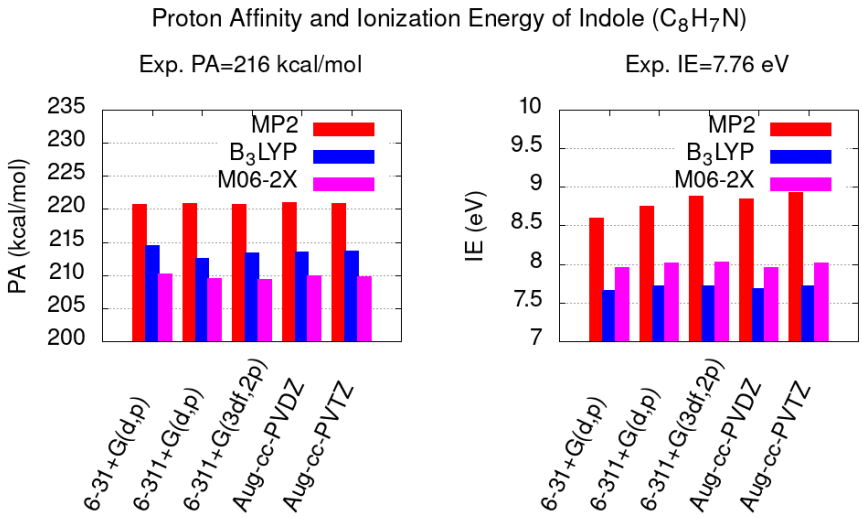

Figure 5: For Table of Contents Only